


# Effect of helium concentration on irradiation damage of Fe-ion irradiated SIMP steel at 300℃ and 450℃

Zhen Yang(杨振), Junyuan Yang(杨浚源), Qing Liao(廖庆), Shuai Xu(徐帅), Bingsheng Li(李炳生)
**Citation:**Chin. Phys. B, 2021, 30 (**5**): 056107. DOI: 10.1088/1674-1056/abd6f9
Journal homepage: http://cpb.iphy.ac.cn; http://iopscience.iop.org/cpb

**What follows is a list of articles you may be interested in**

---

## Degradation of $\beta$-$Ga_2O_3$ Schottky barrier diode underswift heavy ion irradiation

Wen-Si Ai(艾文思), Jie Liu(刘杰), Qian Feng(冯倩), Peng-Fei Zhai(翟鹏飞), Pei-Pei Hu(胡培培), Jian Zeng(曾健), Sheng-Xia Zhang(张胜霞), Zong-Zhen Li(李宗臻), Li Liu(刘丽), Xiao-Yu Yan(闫晓宇), You-Mei Sun(孙友梅)
Chin. Phys. B, 2021, 30 (**5**): 056110. DOI: 10.1088/1674-1056/abf107

## Effect of tellurium ($Te^{4+}$) irradiation on microstructure and associated irradiation-induced hardening

Hefei Huang(黄鹤飞), Jizhao Liu(刘继召), Guanhong Lei(雷冠虹), Ondrej Muránsky, Tao Wei, Mihail Ionescu
Chin. Phys. B, 2021, 30 (**5**): 056108. DOI: 10.1088/1674-1056/abf039

## Evolution of ion-irradiated point defect concentration by cluster dynamics simulation

Shuaishuai Feng(冯帅帅), Shasha Lv(吕沙沙), Liang Chen(陈良), Zhengcao Li(李正操)
Chin. Phys. B, 2021, 30 (**5**): 056105. DOI: 10.1088/1674-1056/abf102

## Comparison of helium bubble formation in F82H, ODS, SIMP and T91 steels irradiated by Fe and He ions simultaneously

Bingsheng Li(李炳生), Zhen Yang(杨振), Shuai Xu(徐帅), Kongfang Wei (魏孔芳), Zhiguang Wang(王志光), Tielong Shen(申铁龙), Tongmin Zhang(张桐民), and Qing Liao(廖庆)
Chin. Phys. B, 2021, 30 (**3**): 036102. DOI: 10.1088/1674-1056/abc2b4

## Structure and tribological properties of Si/a-C:H(Ag) multilayer film in stimulated body fluid

Yan-Xia Wu(吴艳霞), Yun-Lin Liu(刘云琳), Ying Liu(刘颖), Bing Zhou(周兵), Hong-Jun Hei(黑鸿君), Yong Ma(马永), Sheng-Wang Yu(于盛旺), and Yu-Cheng Wu(吴玉程)
Chin. Phys. B, 2020, 29 (**11**): 116101. DOI: 10.1088/1674-1056/ab9c10

---

SPECIAL TOPIC — Ion beam modification of materials and applications

# Effect of helium concentration on irradiation damage of Fe-ion irradiated SIMP steel at 300 °C and 450 °C*

Zhen Yang(杨振)[1,†], Junyuan Yang(杨浚源)[2], Qing Liao(廖庆)[2], Shuai Xu(徐帅)[2], and Bingsheng Li(李炳生)[2,‡]

[1] *Sino-French Institute of Nuclear Engineering and Technology, Sun Yat-sen University, Zhuhai* 519082, *China*

[2] *State Key Laboratory for Environment-Friendly Energy Materials, Southwest University of Science and Technology, Mianyang* 621010, *China*

(Received 8 November 2020; revised manuscript received 16 December 2020; accepted manuscript online 28 December 2020)

SIMP steel is newly developed fully martensitic steel for lead-cooled fast reactors and accelerator-driven systems. It is important to evaluate its radiation resistance via high flux neutron irradiation, where dense He atoms can be formed via (n, $\alpha$) transmutation reaction. Co-irradiation with Fe and He ions, instead of neutron, was performed. Specimens were irradiated with 6.4-MeV Fe ions to the damage dose of 5 dpa at a depth of 600 nm. Three different helium injection ratios of 60-appm He/dpa (dpa: displacements per atom), 200-appm He/dpa and 600-appm He/dpa at a depth of 600 nm, were performed. Two different irradiation temperatures of 300 °C and 450 °C were carried out. The effect of helium concentration on the microstructure of Fe-irradiated SIMP steel was investigated. Microstructural damage was observed using transmission electron microscopy. The formed dislocation loops and bubbles depended on the helium injection ratio and irradiation temperature. Lots of dislocation loops and helium bubbles were homogeneously distributed at 300 °C, but not at 450 °C. The causes of observed effects are discussed.

**Keywords:** martensitic steels, Fe and He co-irradiation, microstructure, transmission electron microscopy

**PACS:** 61.80.–x, 61.80.Jh, 68.37.Lp, 78.40.Kc **DOI:** 10.1088/1674-1056/abd6f9

## 1. Introduction

To reduce the total amount of carbon dioxide in air, it is inevitable to develop clean energies. Nuclear energy, in particular, fusion energy is regarded as one of the candidates. To date, only fission of heavy elements techniques, like uranium, thorium, and plutonium, have been practical applications. Light elements in fusion technology, like deuterium and tritium, are also being actively developed. With a rapid development of fission energy plants in China, more and more nuclear wastes are produced to give many negative influences for human. To dispose long-lived nuclear wastes in deep geological repository is not sustainable in the long term. To satisfy sustainable development of nuclear-power systems, it is urgent to use an effective and secure method to solve the nuclear waste as soon as possible. In 2011, Chine Academy of Sciences proposed a strategic project of advanced nuclear fission energy in the future (named ADS: accelerator-driven system).[1] In this project, a high-power proton accelerator provides a high energy and intense current of proton to collide with spallation target, in order to produce high-intensity neutrons by the (p, n) transmutation reaction. Subsequently, neutron will accelerate transmutation of nuclear wastes to reach two important aims. First, it can greatly improve the fuel burnup, from 3.5%–5% (so far) to 95% (in future). Hence, the limited uranium resource will be used longer. Secondly, the long-lived radionuclide (hundreds of thousands of years) will become short-lived radionuclide (decades), and then these short-lived radionuclides will be easily disposed. Liquid lead-bismuth eutectic (LBE) is regarded as the primary candidate material for spallation target and coolant.[2] Due to a strong corrosion phenomenon when containment materials contact LBE, it is important to reduce corrosion rate of containment materials.[3–5] The formed protective oxide scale on the material surface can prohibit Pb, Bi, and O atoms from penetrating into the substrate. It has been reported that Si element is easy to be oxidized to form a dense oxide scale.[6] Considering the advantage and disadvantage of Si in ferritc-martensitic steels, a new type of reduced activation ferritic-martensitic steel, SIMP steel with 1.4-wt% Si, was cooperatively fabricated by the Institute of Modern Physics, Chinese Academy of Sciences (CAS) and Institute of Metal Research, CAS.[7] Due to strong neutron irradiation and serious LEB corrosion, it is important to evaluate the radiation resistance and corrosion mechanism of SIMP steel. Numerous helium atoms can be formed by the (n, $\alpha$) transmutation reaction. Due to a very low solubility of helium atoms in ferritic-martensitic alloys, helium atoms easily migrate and accumulate into vacancies to form bubbles, which induce helium embrittlement and lattice swelling.[8–12]

*Project supported by the National Natural Science Foundation of China (Grant Nos. U1832133 and 12075194), Sichuan Provial Science and Technology Program, China (Grant No. 2020ZYD055), and the Doctor Research Foundation of Southwest University of Science and Technology (Grant No. 18zx714101).

†Corresponding author. E-mail: yangzh97@mail.sysu.edu.cn

‡Corresponding author. E-mail: libingshengmvp@163.com

© 2021 Chinese Physical Society and IOP Publishing Ltd 

The helium production rate varies from 0.1-appm He/dpa to 100-appm He/dpa (dpa: displacements per atom), based on the intensity of neutron-irradiation.[13] The increase in neutron irradiation will enhance the helium production rate. In ADS system, neutron flux is very large because of the high power of neutron. The helium production rate can reach values of 100-appm He/dpa. The effect of the helium production rate on the microstructure in neutron-irradiated steels is a subject of extensive ongoing research.[14–17] The performance of SIMP steel in radiation environment with high production rates of helium therefore deserves utmost attention. Our recent result showed the irradiation hardness of the Fe and He co-irradiated SIMP steel increases with increasing helium injection ratio at 300-°C irradiation, rather than at 450 °C.[18] So far, the microstructure of Fe and He co-irradiated SIMP steel has not been sufficiently investigated. In this study, we used Fe ions to simulate lattice disorder produced by neutron. Three different helium injection ratios, 60-appm He/dpa, 200-appm He/dpa, and 600-appm He/dpa respectively, were carried out. The lattice disorder was analyzed by transmission electron microscopy (TEM). The present research results are important to enable to evaluate the influence of helium concentration on the evolution of lattice disorder in the application surroundings, such as intense neutron irradiation.

## 2. Experimental process

The nominal chemical composition of SIMP steel is shown in Table 1. The material structure was analyzed by electron backscattering diffraction (EBSD), and the results were present in our previous article (see Fig. 8 in Ref. [18]). SIMP steel has fully martensitic structure with a mean grain size of 1.05 μm.

**Table 1.** Nominal composition of SIMP steel (in unit wt%).

| Steels | Fe | C | Cr | P | Si | V | Mn | Nb | W |
|---|---|---|---|---|---|---|---|---|---|
| SIMP | Bal | 0.2 | 10.7 | 0.004 | 1.4 | 0.2 | 0.5 | 0.01 | 1.2 |

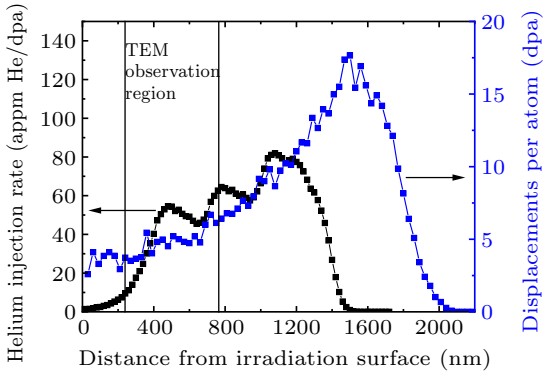



**Fig. 1.** The depth profiles of the displacement damage produced by Fe-ion irradiation and the implanted helium injection rate in Fe–Cr alloys simulated by SRIM-2008. The TEM observation region is located at depths ranging from 250 nm to 750 nm where dense helium atoms are deposited.

The sample was cut into 5 mm × 3 mm × 1 mm dimensions by a wire electrical discharge machining, and then the sample surface was polished by sandpapers and diamond spray to reach mirror polish. Fe and He co-irradiation experiment was performed at the dual-Beam Material Irradiation Facility for Energy Technology (DuET) at the Institute of Advanced Energy, Kyoto University. 6.4-MeV $Fe^{3+}$ ions provided by a 1.7-MeV tandem accelerator with a simultaneous implantation of energy-degraded 1.0-MeV $He^{+}$ ions from a 1.0-MV Singletron Accelerator (the helium beam went through three different thicknesses of aluminum films), in order to provide a uniform distribution of helium atoms in a certain depth range (see Fig. 1). The irradiation temperatures were well controlled at $300 \pm 5$ °C and $450 \pm 5$ °C measured by an infrared thermometer. The fluence of Fe ions was $1.65 \times 10^{16}$ ions/cm$^2$. The Monte–Carlo code Stopping and Range of Ions in Matter (SRIM-2008) quick cascade simulation was used to simulate depth profiles of the Fe irradiation-induced displacement damage and the implanted helium concentration (using the threshold displacement energy of 40 eV and the density of 7.86 g/cm$^3$),[19] as shown in Fig. 1. At a depth of 600 nm, the nominal displacement damage rate and nominal displacement damage were $3 \times 10^{-4}$ dpa/s and 5 dpa, respectively. Three different helium injection ratios, 60-appm He/dpa, 200-appm He/dpa, and 600-appm He/dpa respectively, were performed.

The microstructure of the irradiated sample was observed by a JEOL 2010 TEM operated at 200 kV. A double-tilt holder was used to fulfill kinematical bright-field and dynamical two-beam, as well as weak-beam dark field diffraction conditions. In order to observe damage distribution in depth, cross-sectional TEM samples were prepared. Hitachi 2000 focused ion beam system was used to fabricate cross-sectional TEM samples. After Ga ions thinning, the damage induced by Ga ions during FIB fabrication was removed by electrochemical polishing for 8 ms–15 ms at −45 °C (5% perchloric acid +95% alcohol). The region at depth ranging from 250 nm to 750 nm was characterized by TEM. Convergent beam electron diffraction (CBED) method was used to measure the thickness of observed samples. The size and number density of the observed dislocation loops and bubbles were calculated by the Nano Measurement software. The measurement error is a ±20%.

## 3. Results and discussion

Under the kinematic diffraction condition, the irradiation-induced lattice defects exhibit black contrast. Figures 2(a)–2(c) show that high densities of black spots are observed in the depth range from 250 nm to 750 nm, indicating many lattice defects formed by Fe and He co-irradiation. These lattice defects are almost homogeneously distributed in the observed

region. Except for black spots, many defects exhibiting the elliptical contrast were observed in Figs. 2(a)–2(c). According to the previous report of the ion-irradiated Fe–Cr alloys at temperature 300 °C, most of the observed elliptical defects belong to dislocation loops with Burgers vector of $\boldsymbol{b} = (1/2)\langle 111\rangle$.[20] In addition, the observed black spots can be regarded as the initial growth stage of $(1/2)\langle 111\rangle$ loops. The size distribution and number density of the observed $(1/2)\langle 111\rangle$ loops were measured, and the results are presented in Fig. 4. Besides the observed dislocation loops, many helium bubbles were observed in the damaged region. The formed bubbles are observed under the under-focused condition based on Fresnel contrast.[21] It can be seen that the large and heterogeneous distribution of bubbles in the Fe and He co-irradiated SIMP steel to 60-appm He/dpa, while the small and homogenous distribution of bubbles with increasing the helium injection ratio.

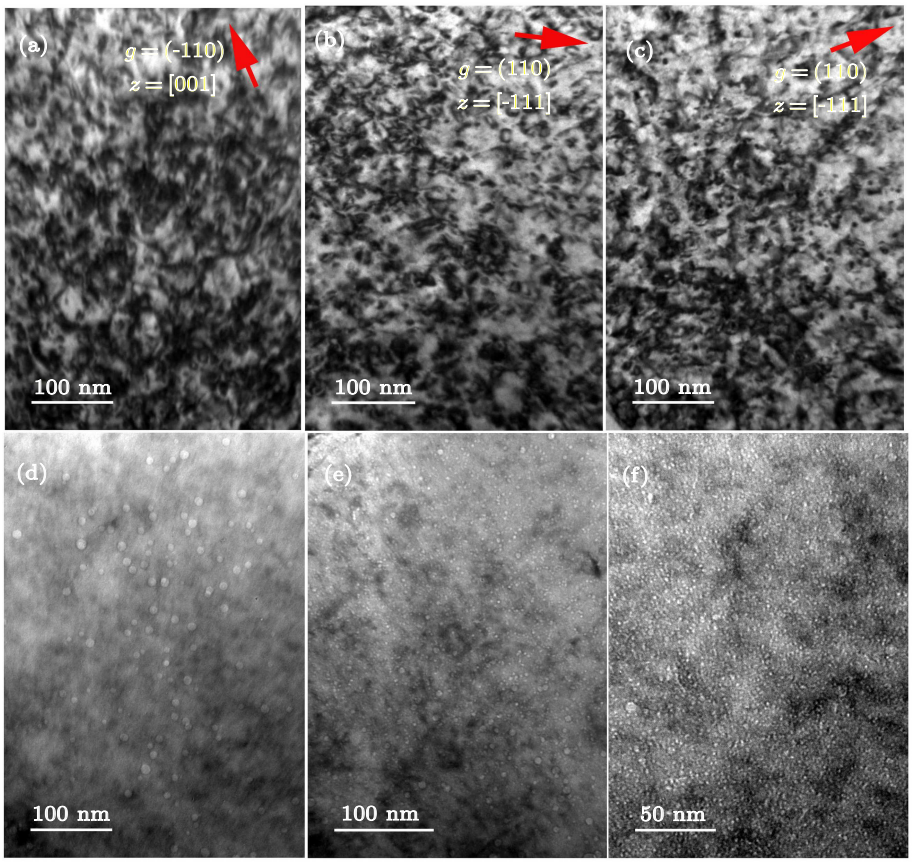



**Fig. 2.** Bright-field XTEM micrographs of irradiation-induced dislocation loops located at depths ranging from 250 nm to 750 nm in the Fe and He co-irradiated SIMP steel at 300 °C to 60-appm He/dpa (a), 200-appm He/dpa, (b) and 600-appm He/dpa (c). Photographs were taken near [001] or [-111] zone axis under the kinematic diffraction condition, $\boldsymbol{g} = (-110)$ or (110). Bright-field XTEM micrographs of bubbles are formed in the Fe and He co-irradiated SIMP steel to 60 appm He/dpa (d), 200-appm He/dpa (e), and 600-appm He/dpa (f). The micrograph was imaged under the under-focused view with $\Delta f = -512$ nm. The sample surface is vertical upward.

Compared to 3000-°C irradiation, the observed dislocation loops after 450-°C irradiation grown significantly. The observed dislocation loops are mixed of $\langle 100\rangle$ loops and $(1/2)\langle 111\rangle$ loops.[20] Many tangled dislocations are observed in Figs. 3(a)–3(c). In addition, a high number of bubbles are observed and these bubbles are inclined to nucleate at dislocations, precipitate-matrix interfaces and grain boundaries, consistent with other reports.[22–24] The heterogeneous distribution of bubbles demonstrates that vacancies rapidly migrate at 450 °C. Vacancies migrate and coalesce into voids, which induce void swelling. It has been reported that the maximum swelling of ferritic-martensitic steels occurs during ion irradiation at near 475 °C.[25] When the helium injection ratio is 600-appm He/dpa, bubble sizes significantly increase. The size distributions of observed dislocation loops and bubbles were measured and the results are given in Fig. 5.

Figure 4 shows the size distribution of observed $(1/2)\langle 111\rangle$ loops and bubbles in the Fe and He co-irradiated SIMP steel at 300 °C to different He injection ratios. It can be seen that the mean sizes of Frank loops and bubbles decrease with increasing the He injection ratio, while the number density of these defects increases, as shown in Fig. 6(a). In particular, a high number density of bubbles was formed after helium injection with 600-appm He/dpa.

Figure 5 shows the size distribution of observed dislocation loops and bubbles in the Fe and He co-irradiated SIMP steel at 450 °C to different He injection ratios. It can be seen that the mean size of dislocation loops is the largest in the Fe and He co-irradiated SIMP steel at 450 °C to 60-appm He/dpa. However, the number density of dislocation loops is the largest in the Fe and He co-irradiated SIMP steel at 450 °C

to 200-appm He/dpa. The number density in the Fe and He co-irradiated SIMP steel at 450 °C to 60-appm He/dpa and 600 appm He/dpa is not obviously different. It should be noted that many tangled dislocations were formed during 450-°C irradiation. This result demonstrates that self-interstitials and vacancies rapidly migrate at 450 °C, resulting in insignificant irradiation hardening.[18] The dislocation loops are not clearly distinguished due to the influence of tangled dislocations.

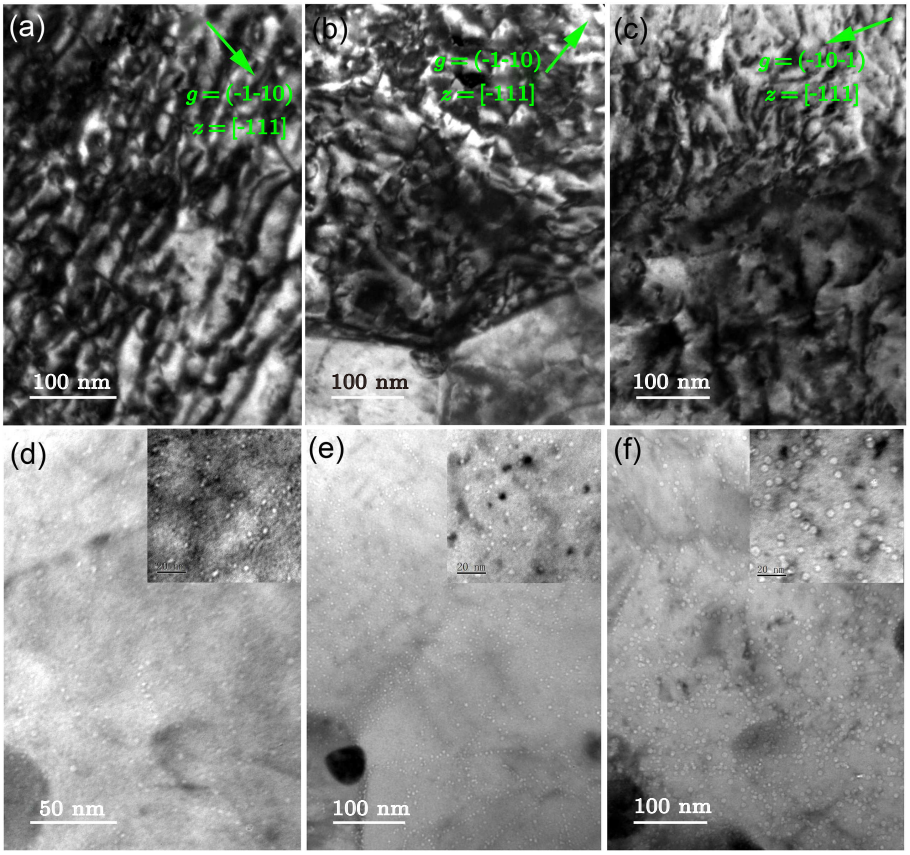



**Fig. 3.** Bright-field XTEM micrographs of irradiation-induced dislocation loops located at depths ranging from 250 nm to 750 nm in the Fe and He co-irradiated SIMP steel at 450 °C to 60-appm He/dpa (a), 200-appm He/dpa (b), and 600-appm He/dpa (c). Photographs were taken near [-111] zone axis under the kinematic diffraction condition, $\boldsymbol{g} = (\text{-}1\text{-}10)$. Bright-field XTEM micrographs of bubbles are formed in Fe and He co-irradiated SIMP steel to 60-appm He/dpa (d), 200-appm He/dpa (e), and 600-appm He/dpa (f). The local areas of images (d), (e), and (f) are magnified as shown in the insets with the same scale of 20 nm. The micrograph was imaged under the under-focused view with $\Delta f = -512$ nm. The sample surface is in vertical upward direction.

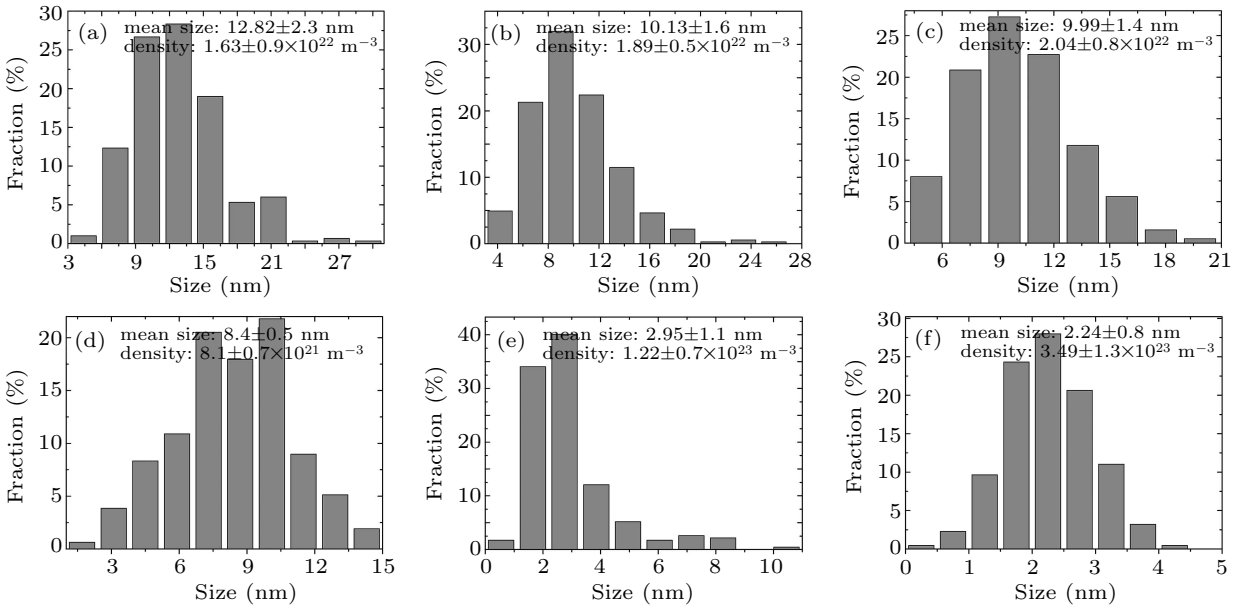



**Fig. 4.** Size distribution of observed dislocation loops in the Fe and He co-irradiated SIMP steel at 300 °C to 60-appm He/dpa (a), 200-appm He/dpa (b), and 600-appm He/dpa (c); size distribution of observed bubbles in the Fe and He co-irradiated SIMP steel at 300 °C to 60-appm He/dpa (d), 200-appm He/dpa (e), and 600-appm He/dpa (f).

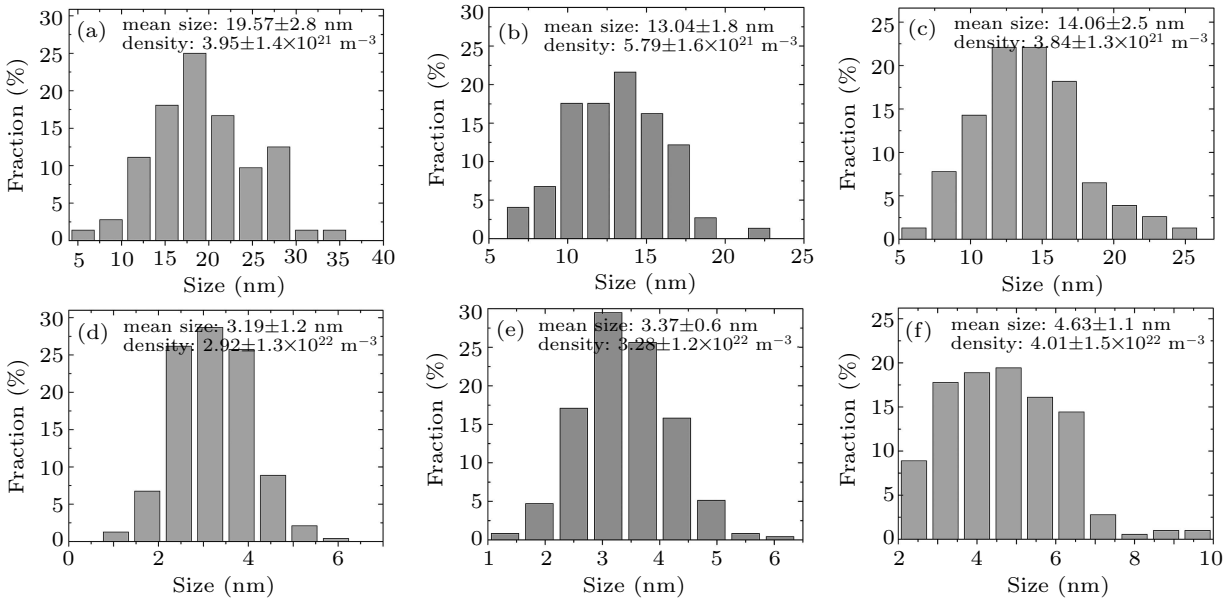



**Fig. 5.** Size distribution of observed dislocation loops in the Fe and He co-irradiated SIMP steel at 450 °C to 60-appm He/dpa (a), 200-appm He/dpa (b), and 600-appm He/dpa (c); size distribution of observed bubbles in the Fe and He co-irradiated SIMP steel at 300 °C to 60-appm He/dpa (d), 200-appm He/dpa (e), and 600-appm He/dpa (f).

Therefore, the measured size and number density of dislocation loops shown in Figs. 5(a)–5(c) only give a general trend. To get a weak kinematic diffraction condition, the sample was tilted to several degrees along $x$ or $y$ axis. In this condition, where dislocation loops and tangled dislocations have weak contrasts, only bubbles are observed under the underfocused condition. The mean size and number density of the observed bubbles increase with increasing the He injection ratio, as shown in Fig. 6(b).

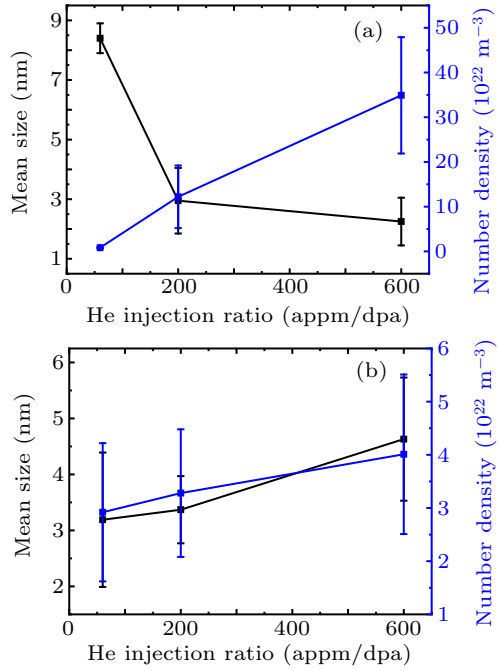



**Fig. 6.** The plot of mean size and number density of observed bubbles as a function of He injection ratio at 300 °C (a) and 450 °C (b).

In comparison between the sample under 300-°C irradiation and the sample under 450-°C irradiation, there are two differences of the microstructure. First, the mean sizes of the observed dislocation loops and bubbles at 300-°C irradiation are smaller than that at 450-°C irradiation, except large bubbles formed in the Fe and He co-irradiated SIMP steel at 300 °C to 60-appm He/dpa. Meanwhile, the number densities of the observed dislocation loops and bubbles at 300-°C irradiation are larger than that at 450-°C irradiation. It has been reported that the change in the number density of He bubble nuclei, $\mathrm{d}N/\mathrm{d}t$, is related to the concentration of He atoms, $c(t)$, where $t$ is time.[26] $\mathrm{d}N/\mathrm{d}t$ increases with increasing $c$, while it decreases with increasing the diffusion coefficient of He atoms. In addition, because the interstitials and vacancies have faster migration rates at 450 °C than at 300 °C, the rapid migration of interstitials and vacancies induced some lattice defect annealing. Other defects grown via absorbing interstitials to form large dislocation loops and tangled dislocations, or absorbed vacancies to form large bubbles. Secondly, the effect of the helium injection ratio on the formation of the observed dislocation loops and bubbles is significant at 300-°C irradiation, rather than at 450-°C irradiation. Due to the low dynamic annealing at 300-°C irradiation, there are many survived irradiation-induced vacancies. Because of the strong binding of He atom with vacancies, these survival vacancies provide positions for helium accumulation to form bubbles.[26] Increasing helium injection ratio, more helium atoms are injected. These helium atoms migrate and accumulate into vacancies to form bubbles. When vacancies are decorated by helium atoms, vacancies will be difficult to migrate.[27] As a result, survived interstitials rapid migrate and coalesce into clusters, such as point defects and dislocation loops, as shown in Fig. 2. At 450-°C irradiation, dynamic annealing is evident, irradiation-induced Frankel pairs recover immediately. Therefore, the number density of the observed dislocation loops de-

creases obviously. However, increasing helium injection ratio to 600-appm He/dpa, some vacancies are decorated by helium atoms, resulting in the increase in survived vacancies. Helium atoms migrate and accumulate into these vacancies to form bubbles. At 450 °C, vacancies can easily migrate and coalesce, resulting in the growth of bubbles with increasing the He injection ratio. In addition, the influence of gain boundaries, precipitate-matrix interfaces, dislocations on the nucleation of bubbles cannot be ignored. The heterogeneous distribution of bubbles formed at 450-°C irradiation can be observed in Figs. 3(d)–3(e). Lots of bubbles are formed along dislocations and in grain boundary planes. The dynamic annealing and the heterogeneous distribution of bubbles induce a weak relationship between the He injection ratio and the formed dislocation loops.

A schematic diagram demonstrating the dislocation loops formed at 300 °C and 450 °C to different He injection ratios is shown in Fig. 7. The mean size of the dislocation loops decreases, while their density increases with increasing He injection ratio at 300-°C irradiation. However, the influence of He concentration on dislocation loops is less pronounced, when Fe and He co-irradiation was performed at 450 °C. The present experimental results demonstrate that the lattice swelling estimated by He irradiation is larger than that of neutron irradiation. However, it is smaller via Fe irradiation than that of neutron irradiation. In addition, the number density of the observed dislocation loops increases with increasing the helium injection ratio at 300 °C, rather than 450-°C irradiation. This result indicates that irradiation hardening increases with increasing the helium injection ratio at 300 °C, which is consistent with our recent report.[18]

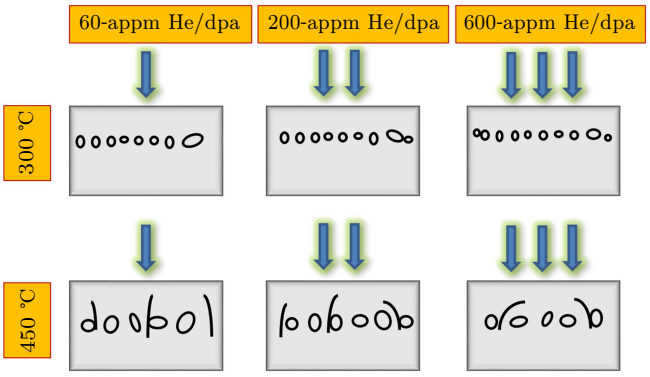



**Fig. 7.** A schematic diagram showing Fe and He co-irradiation-induced dislocation loops at 300 °C and 450 °C to 60-appm He/dpa, 200-appm He/dpa, and 600-appm He/dpa.

## 4. Conclusion

In conclusion, we have investigated the effect of helium concentration on the microstructure of Fe-irradiated SIMP steel at 300 °C and 450 °C to a dose of 5 dpa with 60-appm He/dpa, 200-appm He/dpa, and 600-appm He/dpa respectively. The formed dislocation loops and bubbles were characterized by TEM. The mean sizes of dislocation loops and bubbles decrease, while their number density increases with increasing helium injection ratio when the irradiation was performed at 300 °C. At 450-°C irradiation, the mean size and number density of bubbles increase with increasing helium injection ratio. However, the influence of the helium injection ratio on dislocation loops seems to play only a negligible role.

## References

[1] Zhan W L and Xu H S 2012 *China Academic Journal Electronic Publishing House* **27** 375
[2] Sar F, Mhiaoui S and Gasser J G 2007 *J. Non-Cryst. Solids* **353** 3622
[3] Gong X, Marmy P, Verlinden B, Wevers M and Seefeldt M 2015 *Corrosion Sci.* **94** 377
[4] Gong X, Marmy P and Yin Y 2018 *J. Nucl. Mater.* **509** 401
[5] Liu J, Yan W, Sha W, Wang W, Shan Y Y and Yang K 2016 *J. Nucl. Mater.* **473** 189
[6] Zhang L L, Yan W, Shi Q Q, Li Y F, Shan Y Y and Yang K 2020 *Corrosion Science* **167** 108519
[7] Peng J, Shen T L, Cui M H, Zhu Y B, Li B S, Zhang T M, Li J Y, Jin S X, Lu E Y, Cao X Z and Wang Z G 2019 *J. Nucl. Mater.* **520** 131
[8] Ando M, Wakai E, Sawai T, Tanigawa H, Furuya K, Jitsukawa S, Takeuchi H, Oka K, Ohnuki S and Kohyama A 2004 *J. Nucl. Mater.* **329–333** 1137
[9] Li B S and Dai Y 2014 *J. Nucl. Mater.* **450** 42
[10] Peng L, Huang Q Y, Ohnuki S and Yu C Z 2011 *Fusion Eng. Deg.* **86** 2624
[11] Henry J, Vincent L, Averty X, Marini B and Jung P 2007 *J. Nucl. Mater.* **367–370** 411
[12] Li B S, Wang Z G, Shen T L, Wei K F, Shen Y B, Shibayama T, Lu X R and Xiong A L 2019 *Chin. Phys. Lett.* **36** 046104
[13] Sawan M E 2012 *Fusion Eng. Deg.* **87** 551
[14] Krsjak V, Degmova J, Sojak S and Slugen V 2018 *J. Nucl. Mater.* **499** 38
[15] Degmova J, Krsjak V, Shen T L, Veternikova J S, Gatciova A, Sojak S and Hruska P 2021 *Appl. Surf. Sci.* **538** 148004
[16] Li L, Jin S X, Zhang P, Wang D D, Cao X Z, Guo L P, Xu Q, Li J, Zhang T M, Li L B and Wang B Y 2019 *J. Nucl. Mater.* **526** 151748
[17] Zhu T, Jin S X, Zhang P, Song L G, Jian X Y, Fan P, Zhang X L, Yuan D Q, Wu H B, Yu R S, Cao X Z, Xu Q and Wang B Y 2018 *J. Nucl. Mater.* **505** 69
[18] Li B S, Wang Z G, Wei K F, Shen T L, Yao C F, Zhang H P, Sheng Y B, Lu X R, Xiong An L and Han W T 2019 *Fusion Eng. Deg.* **142** 6
[19] http://www.srim.org
[20] Yao Z, Mayoral M H, Jenkins M L and Kirk M A 2008 *Philosoph. Mag.* **88** 28
[21] Bentzon M D and Tholen A R 1992 *Nanostructured Materials* **1** 229
[22] Liu W B, Ji Y Z, Tan P K, Zhang C, He C H and Yang Z G 2016 *J. Nucl. Mater.* **479** 323
[23] Li Q, Parish C M, Powers K A and Miller M K 2014 *J. Nucl. Mater.* **445** 165
[24] Xia L D, Liu W B, Liu H P, Zhang J H, Chen H, Yang Z G and Zhang C 2018 *Nucl. Eng. Technol.* **50** 132
[25] Wakai E, Sawai T, Furuya K, Naito A, Aruga T, Kikuchi K, Yamashita S, Ohnuki S, Yamamoto S, Naramoto H and Jistukawa S 2002 *J. Nucl. Mater.* **307–311** 278
[26] Trinkaus H and Singh B N 2003 *J. Nucl. Mater.* **323** 229
[27] Sun J J, Li B S, You Y W, Hou J, Xu Y C, Liu C S, Fang Q F and Wang Z G 2018 *J. Nucl. Mater.* **503** 271